Scoping Nuclear Analyses of Shielding Options and Shut Down Dose Rate Contributions in ITER TBSs

M. Harb,[*,a] D. Leichtle,[a] B.Y. Kim,[b] J.P. Martins,[b] J.G. van der Laan,[b] J. Bergman,[b] E. Polunovskiy,[b] and A. Serikov[a]

[a] *Karlsruhe Institute of Technology (KIT)*
Hermann-von-Helmholtz-Platz 1, 76344 Eggenstein-Leopoldshafen, Germany

[b] *ITER Organization (IO)*
Route de Vinon-sur-Verdon, CS 90 046, 13067 St. Paul Lez Durance Cedex, France

[*]Email: moataz.harb@kit.edu

Number of pages: 24
Number of tables: 8
Number of figures: 15

Abstract

One of the advances in the Test Blanket Module (TBM) program [1], within the ITER [2] [3] project, in the last few years concerned the evolution of the Pipe Forest (PF) and Bioshield Plug (BP) designs. In support of the design phase, nuclear analyses to assess several responses in the fusion neutronics environment, inside the Port Interspace (PI) with the existence of the evolved PF and BP, are deemed essential. Nuclear analyses [4] were commenced using the new PF and BP with developing the neutronics models and performing preliminary assessment of the radiation fields and Shut Down Dose Rate (SDDR) in the PI. In this paper, the results of a full suite of nuclear analyses are discussed, which covers more configurations and radiation sources, in two plasma operational modes: on and off. For the plasma-on mode, different shielding options were examined. The results showed a clear benefit of combining the installation of shielding panels on the PF enclosure with those in the BP "dogleg", through which the pipes penetrate to the Port Cell (PC) area. For the plasma-off mode, SDDR was assessed from different sources: activated components and residual LiPb layers in pipes after drainage. As maintenance operations are foreseen during the lifetime of the facility, the SDDR was also assessed for access conditions, open BP doors, and transport conditions, with PF extracted in gallery.

Keywords — ITER, TBS, Neutronics, Shielding, Shutdown dose rate

I. INTRODUCTION

The ITER [2] [3] project has seen major advances in the last few years both on the design front as well as on the ground. The ITER site has seen the delivery of many components; such as few Toroidal Field (TF) coils and Vacuum Vessel (VV) sectors from manufactures in the member states, also the lowering the bottom part of the cryostat into the ITER Tokamak pit. Different ITER design teams have been making progress in producing high fidelity models of different components that will be installed in the facility. In support of the design efforts and iterations, the nuclear behavior of the different components in the fusion neutronics environment has to be assessed. Such a feedback/input is important not only for mechanical/structural design of the components, but also for material validation as residual activities are of prime importance for maintenance operations and waste classification for storage/disposal.

In ITER, a Test Blanket System (TBS) [1] consists of a Test Blanket Module - Port Plug (TBM-PP) and its associated systems. Subsequently, the TBM-PP consists of a TBM-Frame and two TBM-Sets (or two Dummy-TBMs). Two TBSs will be installed in two equatorial ports in the ITER facility. As part of the design plan, a TBM-PP with two Dummy-TBMs should be available to replace the original TBM-PP as backup, and in turn should provide the same shielding performance for both the Port Interspace (PI) and the Port Cell (PC). In a previous study [5], the TBM-PP (with two Dummy-TBMs) was the subject of extensive nuclear analyses that assessed the radiation fields, Shut Down Dose Rate (SDDR), and residual activities after shutdown. Since then, the Pipe Forest (PF) has gone through an evolution of the design; concerning the routing of pipes, the PF structure, and the inclusion of a water Delay Tank (DT); as well as the Bioshield Plug (BP).

In this paper, the results of extensive nuclear analyses performed using the evolved PF and BP are discussed. The main focus of this work will be on three main topics: shielding options in the PF and BP, assessment of SDDR contributions from different radiation sources, and assessment of SDDR for maintenance operations. In section II, a brief overview of the neutronics model will be given, as well as a detailed description of the different radiation sources. The different methods/tools used in this work will also be introduced in that section. In section III, the results from comparative nuclear analyses of the different shielding options will be discussed with a focus on the BP performance. Section IV will be dedicated to highlight the dose in Si which is relevant

for electronic components that might be present in the PI. Sections V, VI, and VII will be dedicated to the assessment of the SDDR. Finally, conclusions will be presented in VIII.

II. MATERIALS AND METHODS

II.A. Neutronics Model

In order to assess the effect of the design evolution of the different components in the PF and BP, an accurate representation of the PF+BP model and the fusion environment, at large, has to be ensured. In the analysis activities commenced in late 2019 [4], the PF+BP neutronics model was developed, the details of which are given in [4] and described briefly hereafter. The isolated model of the TBS within the ITER tokamak (up to the bioshield) consists of the TBM-PP, with two identical Dummy-TBMs and a TBM frame, and the developed model of the PF+BP. The TBM-PP model was refurbished from a previous analysis [5], since no design changes has been made since then. The model retained a high level of details of the internals of the TBM-PP and the dummies, with accurate representation of the water cooling pipes.

The clean Computer Aided Design (CAD) model of the PF+BP was converted to MCNP [6] input representation. The model contained a detailed representation of the pipe work, pipes support, PF structure, water delay tank, thermal insulation of the pipes, BP doors, and central BP. A full description of the simplifications and materials used can be found in [4]. To represent the fusion environment, the reference MCNP 40^{o} sector model, C-Model [7] [8] was used. The TBM-PP and PF+BP models were then integrated into C-Model in equatorial port #16, replacing the generic filler in that port. Models of the correct port environment in upper, lower and lateral equatorial ports were also integrated to replace the generic fillers [9]. The neighboring ports included models of the port plugs for the Electron Cyclotron (EC) and Ion Cyclotron (IC) heating systems in the upper and equatorial ports. A representation of the cryopumps was also integrated in the lower port.

In this paper, different variations of the baseline configuration of the PF and BP are used to perform comparative nuclear analyses. The baseline configuration, designated as C3RA, is a **R**eference configuration with water present in the Water Cooling System (WCS) in both the TBM-PP and PF, LiPb present in the LiPb circuit in the PF, a delay tank filled with water, and full thermal insulation, option **A**, of pipes passing through the BP dogleg. The other configurations,

variants of C3RA, are listed in Table I. It is worth noting that in all configurations the water and LiPb are fully drained out during plasma-off mode, for SDDR calculation. The BP butterfly doors are closed for both plasma-on and -off modes for all configurations except for C3OB, where the access conditions after shut down are investigated.

TABLE I
Different PF and BP Configurations

Description	Configuration				
	C3RA	C3EI	C3EX	C3RB	C3OB
Water in TBM-PP and PF	x	x	x	x	
LiPb in LiPb circuit	x	x	x	x	
External PF structure shielding		x	x		
Internal PF structure shielding		x			
BP dogleg full thermal insulation, option A	x	x	x		x
BP dogleg shielding, option B				x	
Closed BP doors	x	x	x	x	

The CAD model of the TBM-PP, PF, and BP is shown in figures 1 with all materials identified. Figure 2 shows the same model but with the PF structure, peripheral BP, and TBM-PP frame removed. It is worth mentioning that in the figures BHC stands for Borated Heavy Concrete which is used for the fillers of the BP. In the C3RA variant configurations, different thicknesses of shielding panels are used: 5 cm in the BP dogleg, 2 cm for the external PF structure, 2 cm for the internal panel facing the rear side of the TBMP-PP, and 0.5 cm for those lining the maintenance corridor.

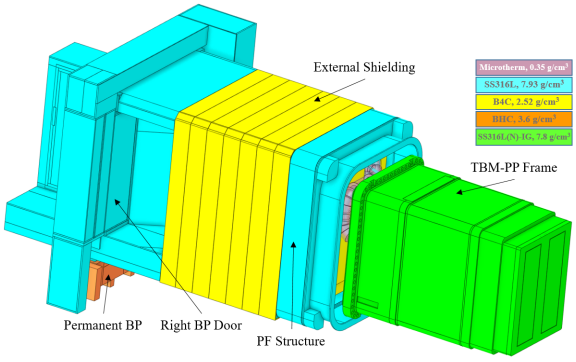

Fig. 1. CAD Model of the TBM-PP, PF, and BP

II.B. Analysis Tools

The transport calculations were performed using D1SUNED v3.1.4 [10] code. For plasma-on mode, the FENDL3.1d nuclear cross sections library was used, while for SDDR calculation,

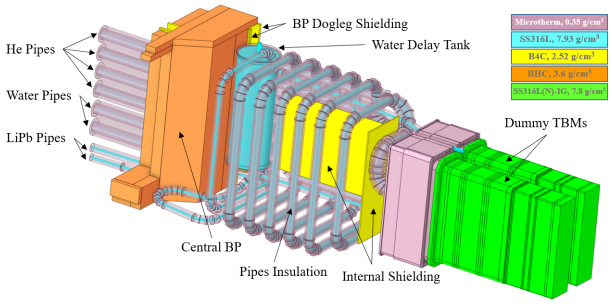

Fig. 2. CAD Model of the Internal Components of the TBM-PP, PF, and BP

plasma-off mode, the D1SUNED custom data library was used instead along with ICRP-74 [11] flux-to-dose-rate conversion factors. Due to the heavy attenuation of neutrons and gammas in traversing the TBM-PP and the PI, Weight Windows (WW) generated using ADVANTG [12] were used for both plasma-on and -off modes. All transport calculations were performed on MARCONI HPC cluster [13]. For activation calculations, the nuclear inventory analysis code FISPACT-II [14] was used along with EAF2010 library.

The neutron and gamma fluxes and SDDR distributions in the PI were obtained over a superimposed 5 x 5 x 5 cm^3 mesh. The SDDR was also calculated at six human-sized tallies, 40 x 60 x 190 cm^3, placed at the TBM-PP - PF interface, along the maintenance corridor, and behind the BP, as shown in figure 3, which represents a horizontal cross section of the CAD model of the TBM-PP, PF, and BP. The BP performance was assessed using two, 10 cm thick and 30 cm away, tallies behind the BP. A central tally is located opposite the central BP while the remaining extent to the port walls is covered by a peripheral tally, as shown in figure 4. The total tally in figure 4 is also 10 cm thick and covers the full extent, behind the BP, to the port walls.

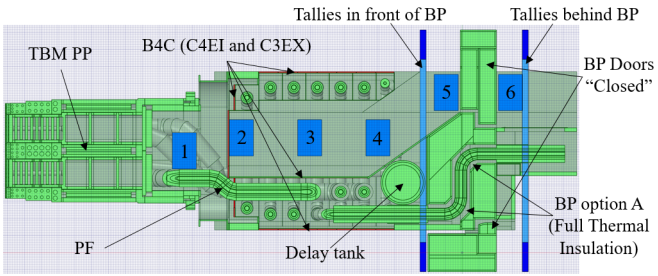

Fig. 3. 1 - 6 Human-Sized and BP Tallies in the PI

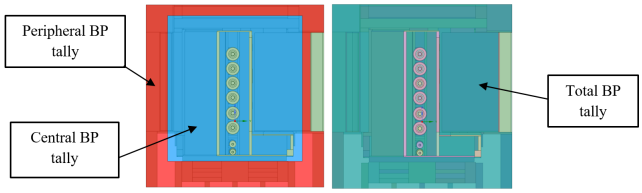

Fig. 4. BP Tallies

II.C. Sources

II.C.1. Plasma

The standard ITER plasma neutron source defined in C-Model [8] was used for the neutron transport simulations in the plasma-on mode. The source describes a standard deuterium–tritium (D-T) campaign with 500 MW of fusion power and a neutron emission rate of 1.77 x 10^{20} n/s, which translates for the 40° sector of the C-Model to a source strength of 1.973 x 10^{19} n/s.

II.C.2. Activated Water

The cooling water flowing through the pipes in the PF and the TBM-PP will be activated due to ^{16}O(n, p)^{16}N and ^{17}O(n, p)^{17}N reactions. ^{16}N decays by gamma emission yielding 7.12 MeV (5%) and 6.13 MeV (68.8%), while ^{17}N decays by emitting neutrons with 1.69 MeV (6.9%), 1.16 MeV (49.8%) and 0.386 MeV (37.7%). It can be seen that the gamma spectrum from ^{16}N is hard and has to be taken into account for plasma-on mode, especially for Si dose in electronics in the PI. Due to the low energy of emitted ^{17}N decay neutrons, it is not expected to have a large impact in the PI but it needs to be accounted for regarding the total neutron flux behind the BP.

Using the results from previous analysis on the average activity density of cooling water in the TBM-PP [15], the emission densities of decay gamma and neutrons from ^{16}N and ^{17}N in the PF were calculated. This was achieved by segmenting the hot leg pipe, the one carrying water from the TBM-PP side to the PC area, and assign an average activity to each segment based on the calculated inlet and exit activity of each according to the radioactive decay of ^{16}N and ^{17}N. Scoping analysis showed negligible production of ^{16}N and ^{17}N in the PF in comparison to the emission densities from the source in water coming from the TBM-PP, therefore it was not accounted for. The key parameters used in the source evaluation are given in table II and the activities in the pipe segments are plotted in figure 5. It can be seen by comparing the inlet

and exit activities of the delay tank that it reduces the activity density by 2 and 3 orders of magnitude for ^{16}N and ^{17}N, respectively. A dedicated script was then used to generate MCNP source definitions using the calculated segments activities.

TABLE II
Activated Water Source Parameters

Parameter	^{16}N	^{17}N
PF		
Activity entering from TBM-PP [Bq/cm^3]	5.5 x 10^9	7.0 x 10^5
Water flow rate [cm^3/s]	6.0 x 10^3	
Mass flow rate [kg/s]	4.2	
Inner pipe diameter [cm]	7.366	
Delay Tank		
Residence time [s]	33	
Water volume [cm^3]	4.8 x 10^5	
Inlet activity [Bq/cm^3]	2.27 x 10^9	1.54 x 10^5
Exit activity [Bq/cm^3]	9.17 x 10^7	6.39 x 10^2
Assigned activity [Bq/cm^3]	1.18 x 10^9	7.73 x 10^4
PF + Delay Tank		
Source strength [s^{-1}]	7.66 x 10^{14}	5.12 x 10^{10}

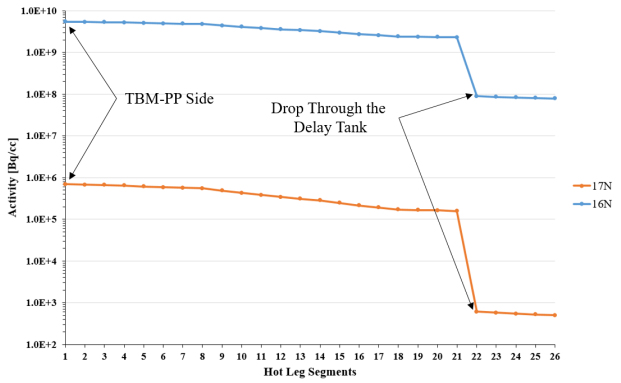

Fig. 5. Activity Density [Bq/cm^3] of ^{16}N and ^{17}N

II.C.3. Activated Residual LiPb

In case of a TBM-PP design with a TBM set that utilizes the LiPb eutectic alloy to serve as breeder/multiplier, during plasma operation the LiPb will be pumped through the LiPb circuit, in the TBM-PP and PF. LiPb will experience the highest levels of neutron flux at the TBM-PP and in interacting with neutrons it becomes a source of radiation as it circulates in the PI [16]. A matter of concern is the expected residual layer of LiPb in the PF after shutdown of the facility. While LiPb will be drained out after shutdown, a thin residual layer is expected to adhere to the

inner surface of the LiPb pipes. This residual layer will become a source of decay gammas in the PF. While the model used in this study, described in subsection II.A, doesn't contain the actual model of a TBM set with LiPb, it still can be used to assess the SDDR in the PF due to residual activated LiPb. This is driven by the necessity to address all sources of radiation in the PF to help the design iterations of the different components in that region.

The LiPb used in this analysis [4] has a density of 9.7 g/cm^3, is 90% enriched in ^{6}Li, and contains about 0.001 weight % Nb. In order to accurately build up the correct inventory of isotopes, the neutron spectrum was tallied in the PF to be used for FISPACT activation calculation to obtain the gamma emission density and spectrum. Because LiPb flowing in pipes will see different levels of irradiation, a LiPb-volume-averaged total neutron flux, 4.47 x 10^{13} n/cm^2/s, was used for normalization. That value corresponds to the average neutron flux that the LiPb will encounter in flowing through the TBM-PP and PF. The last pulse in the Short irradiation scenario, will be discussed in V, was modified by using the total neutron flux in the PF only as the normalization. This was necessary to build up the correct inventory at shut down, end of the irradiation phase.

To assess the impact of a residual activated LiPb layer in the PF, several layer thicknesses were considered. The MCNP source definition was then generated using a dedicated script that produced the distribution on the inner surface of the LiPb pipes. The residual LiPb layer is assumed to be uniform on the inner surface of the pipe. The important parameters used for source generation are listed in table III. The maximum decay gamma energy, emitted from activated LiPb, is in the range 4-5 MeV and the overall emission probability is skewed towards lower energies, below 1 MeV. Figure 6 shows the starting positions, as green dots, of 10^4 sampled particles in MCNP from the generated LiPb source. It can be seen that a large fraction of the total decay gammas are emitted near the BP where a lot of pipe work of the LiPb circuit exist. In section V.B, the SDDR due to the different residual thicknesses will be presented.

TABLE III
Residual LiPb Parameters at 12 Days of Cooling Time

Layer Thickness [mm]	0.1	0.5	1
Original LiPb Volume in Pipes [cm^3]	3.01 x 10^4		
Residual Volume Fraction	0.00976	0.0483	0.09541
Residual Mass in Pipes [g]	2.79	13.81	27.28
Residual Layer Cross Sectional Area [cm^2]	0.1282	0.6346	1.2535
Activity per Unit Length [Bq/cm]	1.35 x 10^6	6.67 x 10^6	1.32 x 10^7
Source Strength [γ/s]	3.09 x 10^9	1.53 x 10^{10}	3.02 x 10^{10}

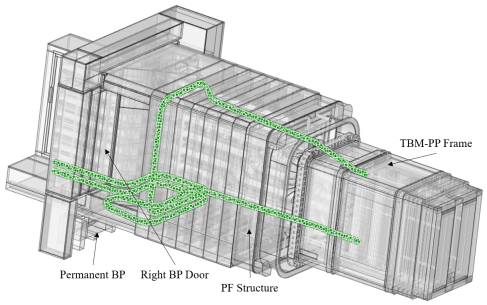

Fig. 6. Starting Positions of 10^4 Gammas in MCNP from Activated LiPb

III. PLASMA-ON MODE: SHIELDING

III.A. Plasma Neutrons

The first set of analyses targeted comparing the effect of the different proposed shielding options on the neutron flux distribution in the PI. The proposed shielding options included: internal and external B_4C panels in the PF structure - C3EI, external only B_4C panels in the PF structure - C3EX, and B_4C panels lining the pipe penetration in the BP dogleg - C3RB. It is worth mentioning that, for all configurations, the neutron transport simulations were conducted with at most 8.0 x 10^{-7} lost particles rate, which is generally considered as acceptable. Figure 7(a) shows a mapping of C3RA total neutron flux distribution in the PI at the horizontal midplane of the port. The neutron flux is reduced by five orders of magnitude after traversing the TBM-PP and by an additional two orders of magnitude behind the BP, compared to the rear side of the TBM-PP.

Figure 7 shows mapping of the relative decrease in the total neutron flux of C3EI, C3EX, and C3RB, in comparison to C3RA. The mapping was obtained by calculating the relative decrease, voxel-wise, over the neutron flux mesh. The artifacts around the TBM-PP and behind the BP are statistical in nature, due to differences in convergence, and should be ignored. In Figure 7(b), C3EI, we see a decrease of almost 60% in the PI, inside the maintenance corridor and a decrease of about 40% near the right BP door. This is the direct impact of the shielding panels blocking neutrons coming from the TBM-PP rear side, via the internal shielding panel facing it, and from neighboring ports, via the external panels lining the PF structure from the outside. The direct impact of the removal of the internal shielding panels in C3EX can be inferred from figure 7(c) where less reduction can be seen behind the maintenance corridor door that faces the TBM-PP rear side, almost 40% compared to almost 60% for the C3EI configuration.

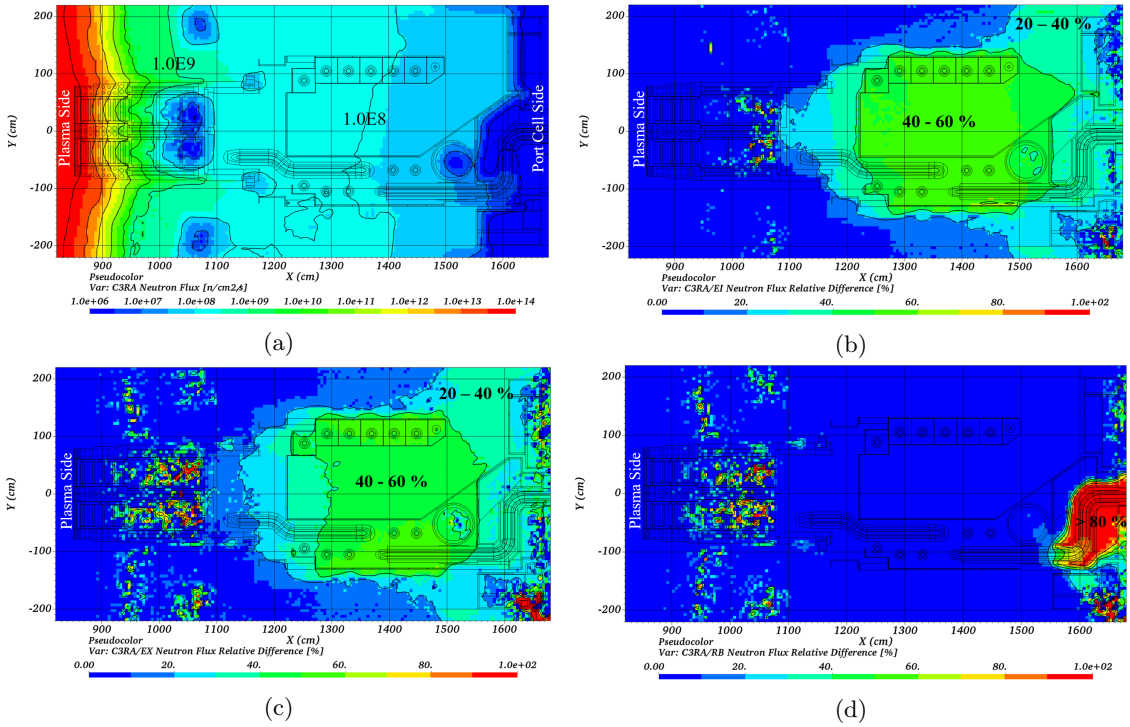

Fig. 7. (a) C3RA Total Neutron Flux [n/cm^2/s] and the Relative Neutron Flux Decrease in (b) C3EI, (c) C3EX, and (d) C3RB, in Comparison to C3RA

As the neutron flux levels will be directly linked to the SDDR, since activation of components will depend on the neutron flux magnitude and energy distribution, it is recommended to use the external and internal shielding option to better shield the maintenance corridor, and help reduce structure activation especially near the TBM-PP rear side. In figure 7(d), lining the BP dogleg pipe penetration with shielding panels helps reduce the total neutron flux levels along the penetration and behind the central BP by about 80%. This shielding option is then a strong candidate to mitigate any high neutron flux levels in the PC behind the BP.

III.B. BP Performance

The BP performance can be assessed in two ways; by mapping the total neutron flux behind the BP and by comparing the values for the central and peripheral, figure 4, tallies for all shielding options. Figure 8 shows a mapping of the total neutron flux behind the BP for C3RA configuration. Few regions behind the BP have locally elevated flux levels compared to their respective surrounding areas. Those regions were found to be; the clearance above the door, around the

thermal insulation of pipes penetrating the BP dogleg, and under the central BP. Of all of those, the region that needs attention is the area under the central BP. This part of the permanent BP contains vents and in some parts it was found that the thickness of the BHC to be less efficient in blocking neutrons. Hence, the local increase in the flux. Since then, the BP has been revised and analyses are now ongoing to assess the improved design to assure compliance with the flux limit behind the BP. The values of the BP tallies for C3RA are listed in table IV and it can be seen that, with the local increase in the flux, that the central tally behind the BP is below 6.0 x 10^4 n/cm^2/s, the limit behind the BP.

TABLE IV
Total Neutron Flux [n/cm^2/s] (MCNP Relative Error) in BP Tallies

	Central behind BP	**Peripheral behind BP**	**Total behind BP**
C3RA	2.55 x 10^4 (0.01)	4.07 x 10^4 (0.01)	3.15 x 10^4 (0.01)
C3EI	1.84 x 10^4 (0.05)	3.12 x 10^4 (0.13)	2.35 x 10^4 (0.06)
Ratio (C3EI/C3RA)	0.72	0.77	0.74
C3EX	1.85 x 10^4 (0.05)	3.07 x 10^4 (0.03)	2.33 x 10^4 (0.06)
Ratio (C3EX/C3RA)	0.73	0.76	0.74
C3RB	1.58 x 10^4 (0.01)	3.79 x 10^4 (0.02)	2.45 x 10^4 (0.01)
Ratio (C3RB/C3RA)	0.62	0.93	0.78

In continuation to the discussion on the efficacy of the different shielding options in III.A, the values of the total neutron flux in the BP tallies are compared, as listed in table IV. The most effective shielding option to reduce the neutron flux behind the BP is C3RB, using shielding panels lining the dogleg pipe penetration. It results in a reduction of 38% in the central tally. The other options, C3EI and C3EX, also provide some reduction in the neutron flux of almost 27%. Combining both options, C3RB and C3EI, would help reduce the neutron flux behind the BP, as well as reduce activation of components in the maintenance corridor. Hence, lowering the prospective SDDR levels in the corridor for maintenance operations.

III.C. ^{17}N Decay Neutrons

Using the ^{17}N decay neutron source, described in II.C.2, neutron transport simulation was conducted using configuration C3RA to obtain the neutron flux distribution in the PI as well as the values of the BP tallies. Mapping of the neutron flux in the PI is shown in figure 9 and it can be seen that the delay tank is the major source of decay neutrons, causing an increase in the neutron flux in the central BP as well as behind the BP. It is worth noting that the MCNP relative error in the PI is below 10%.

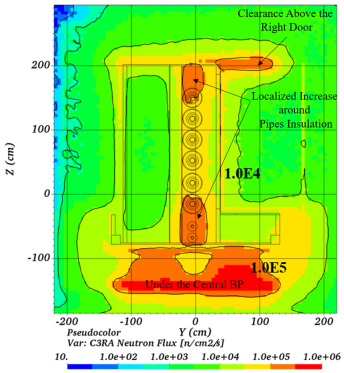

Fig. 8. C3RA Total Neutron Flux [n/cm^2/s] behind the BP

In comparison to figure 7(a), the neutron flux due to water activation is about three orders of magnitude lower, also the spectrum is softer as discussed in II.C.2. Hence, ^{17}N decay neutrons are not expected to cause an increase in components activation nor to impact the SDDR levels in the PI. However, behind the BP, where the plasma neutron flux level is low, it will play a major role! Table V lists the values of the tallies behind the BP. Accounting for plasma and ^{17}N decay neutrons, the central tally behind the BP slightly exceeds the limit! This can be easily mitigated by implementing the C3RB shielding option which would result in a significant reduction in the flux levels behind the BP.

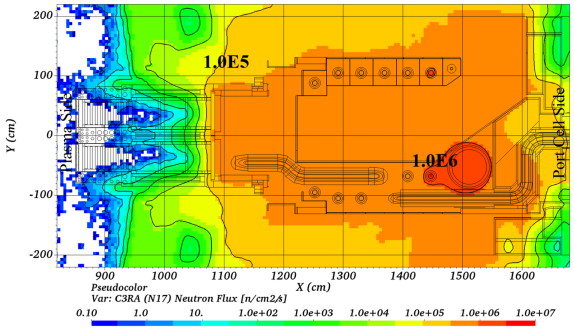

Fig. 9. C3RA Total Neutron Flux [n/cm^2/s] due to ^{17}N Decay

TABLE V
C3RA Total Neutron Flux [n/cm^2/s] (MCNP Relative Error) in BP Tallies

	Central behind BP	**Peripheral behind BP**	**Total behind BP**
Plasma neutrons	2.55 x 10^4 (0.01)	4.07 x 10^4 (0.01)	3.15 x 10^4 (0.01)
^{17}N decay neutrons	4.24 x 10^4 (0.001)	1.13 x 10^4 (0.001)	3.01 x 10^4 (0.001)
Total	6.79 x 10^4 (0.002)	5.14 x 10^4 (0.011)	6.16 x 10^4 (0.003)

IV. DOSE IN SI

The radiation dose in Si, due to both neutrons and gammas, is an important nuclear response because electronic equipment will be present in the PI, either for monitoring or diagnostic purposes. Several simulations were conducted, on the C3RA configuration, to assess the dose in Si. The analyses involved assessing the dose distribution in the PI due to neutrons, from plasma as well as from ^{17}N decay. The dose due to gamma was also assessed, due to prompt gamma produced by plasma neutron interactions, and decay gamma emitted from ^{16}N in activated cooling water.

In the PI, plasma neutrons caused dose in Si was found to be lower than 0.01 Gy/hr, similarly for ^{17}N decay neutrons. Also, prompt gamma dose in Si was found to be lower than 1 Gy/hr. On the other hand, the dose in Si due to ^{16}N decay gamma was found to be the dominant of them all, a mapping is shown in figure 10. The dose was obtained using the ^{16}N decay gamma source described in II.C.2. The dose in Si in the maintenance corridor is as high as 100 - 1000 Gy/hr. As a result, the gamma flux and the dose in Si due to activated water should be paid attention to for all considerations of electronics in the PI, especially during plasma-on mode.

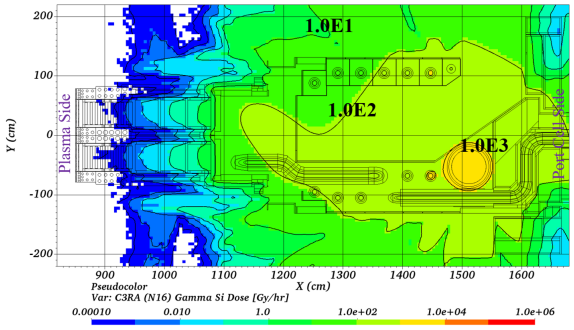

Fig. 10. C3RA ^{16}N Decay Gamma Dose in Si [Gy/hr]

V. PLASMA-OFF MODE: SDDR

The current scoping nuclear analyses are conducted in support of the conceptual designs of the PF and BP and one of the key nuclear responses is the SDDR during maintenance. ITER is expected to have a series of operational campaigns; a single First Plasma (FP), two pre-Fusion Plasma Operation (PFPO), and eight Fusion Plasma Operation (FPO). During the FPO campaigns, the TBM is expected to get swapped every two years, after each campaign. ITER reference irradiation

scenario for the TBM program is called the Short scenario, which captures the irradiation of the TBM-PP, frame and TBM-set, after being swapped during operation. The Short scenario spans 4 years of operation with varying fusion power and ends with several pulses followed by proper dwell times; 17 pulses at 500 MW and 3 pulses at 700 MW. The last three pulses account for an enhanced plasma operation beyond the nominal 500 MW mode. This has been adopted to envelope the short term activities immediately after cessation of plasma burn.

V.A. Activated components

Using the model of the TBM-PP, PF, and BP integrated into C-Model, as described in II.A, SDDR calculations were performed with all cooling fluids and LiPb drained out and with the BP doors remain closed. The SDDR was obtained for several cooling times but here the focus will be on the 12 days after shut down, since maintenance operations are not expected to start before that. During operation, neutrons from the plasma impinge on the equatorial port and interact with the materials present in the TBM-PP, PF, and BP. Those nuclear reactions often lead to transmutation of the nuclides, eventually generating decay gamma emissions from radioactive products. The biological dose due to decay gamma, from activated components, is then the primary focus as maintenance operations have to be planned accordingly involving personnel access.

Using the short irradiation scenario, the SDDR distribution in the EP was obtained as shown in figure 11. The MCNP relative error is $< 15\%$ in the PI. From the figure, it can be seen that the SDDR due to plasma neutron activated components is < 100 μSv/hr. As workers are expected to carry out maintenance activities inside the corridor within the PF area, in the maintenance corridor, the SDDR was also calculated for the human-sized tallies, figure II.B, and listed in table VI. As expected, the highest dose is delivered at positions 2 and 3 located inside the maintenance corridor where the worker is surrounded by the activated components from all sides. For C3RA, the SDDR due to activated components due to ^{17}N decay neutrons was also assessed. It was found that the SDDR in the PI and in all of the 6 tally locations is less than 0.12 μSv/hr, table VIII.

The efficacy of the different shielding options can also be deduced from the results listed in table VI. The real impact of not adding the internal shielding panels can be seen inside the maintenance corridor, at tallies 2 and 3, by comparing the results for C3EI and C3EX. Keeping

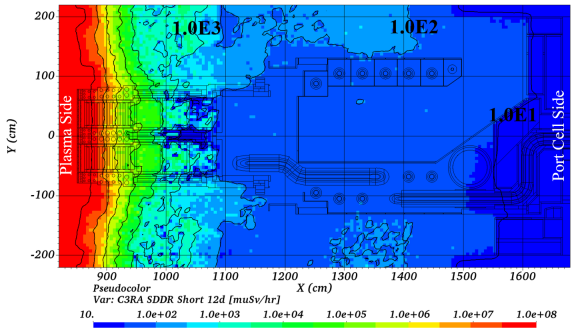

Fig. 11. C3RA SDDR [μSv/hr] at 12 days after Shut Down

TABLE VI
SDDR [μSv/hr] (MCNP Relative Error) at 12 days after Shut Down

Tally No.	C3RA	C3EI	C3EX	C3OB
1	70.68 (0.01)	41.48 (0.02)	48.76 (0.03)	74.47 (0.03)
2	78.44 (0.01)	27.97 (0.01)	38.13 (0.03)	84.27 (0.04)
3	79.87 (0.01)	27.98 (0.01)	33.23 (0.02)	90.33 (0.08)
4	61.89 (0.01)	21.39 (0.01)	24.76 (0.02)	67.13 (0.06)
5	40.42 (0.01)	19.15 (0.01)	21.16 (0.01)	33.00 (0.03)
6	0.01 (0.02)	0.01 (0.04)	0.01 (0.05)	7.93 (0.04)

in mind that the results in the table are only due to activated components, and expecting an increase in the values after adding contributions from residual LiPb, it is highly recommended to use external and internal shielding option. This approach will help reducing the SDDR inside the maintenance corridor by more than 50%.

V.B. Activated Residual LiPb

Using the MCNP generated sources for each of the studied cases of layer of thicknesses: 0.1, 0.5, and 1 mm, SDDR was calculated in the PI. Figure 12 shows a mapping of the SDDR after 12 days following shut down due to a 0.1 mm thick residual layer in the base configuration, C3RA. The MCNP relative error is less than 1% in the PI. A local increase in SDDR levels, compared to the rest of the PF, can be seen around the delay tank with values larger than 80 μSv/h around the LiPb pipe. In contrast to the SDDR from activated components, figure 11, the LiPb pipes penetrating the BP and exiting to the PC area causes an increase in the SDDR behind the BP. Table VII lists the values of the six human-sized tallies for the three thicknesses of residual LiPb layers.

Keeping in mind that an assumption of a uniform layer on the inner surface of the pipes went

into producing the source, the table nonetheless gives a measure of the sensitivity of the SDDR levels to the thickness. We can see that an increase from 0.1 to 0.5 mm thickness in residual LiPb can cause the SDDR levels to quadruple! As a result, the issue of activated residual LiPb in the PF has to be given a thorough investigation, by dedicating experiments to test the distribution and thickness of such layer and investigate ways to mitigate its impact, or even reduce its thickness.

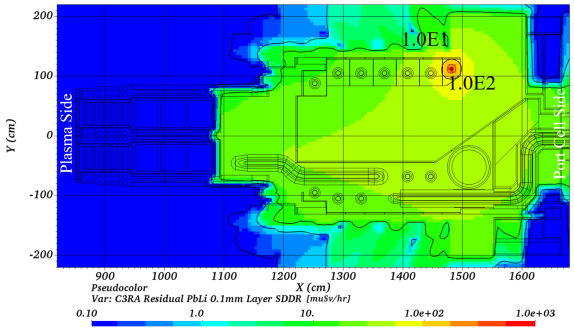

Fig. 12. C3RA SDDR [μSv/hr] due to Residual 0.1 mm LiPb Layer

TABLE VII
Residual Activated LiPb SDDR [μSv/hr] at 12 Days

Tally No.	Residual Activated LiPb Layer		
	0.1 mm	**0.5 mm**	**1 mm**
1	39.69	196.48	388.10
2	27.70	137.13	270.86
3	35.43	175.44	346.53
4	58.58	290.02	572.85
5	35.91	177.79	351.19
6	6.94	34.38	67.91

VI. PLASMA-OFF MODE: MAINTENANCE

Maintenance operations are foreseen at different operational stages during the lifetime of a complex facility like ITER. With a large number of integrated engineering systems, the design process of any individual component is not an isolated process and has to take into consideration the maintenance scenarios to repair or replace the component. As a result, there is a tightly closed feedback loop between design, operation, and maintenance of the facility. As briefly introduced earlier, the TBM set is foreseen to be swapped after every campaign, approximately 2 years. Considering maintenance operations, the steps can be imagined as follows: shutdown, cooling down of the PF and TBM sets in-place, opening the BP doors, accessing the PI or removing the

PF to the gallery behind the BP. The projected duration of such a process is 12 days following the shut down. As a result, access conditions to the PI and the radiation levels around an isolated PF are of prime importance for maintenance operations.

VI.A. Access Conditions

In order to simulate the opening of the BP door after shut down, the SDDR was calculated over two separate steps. The first step involved obtaining the decay gamma source distribution of the closed door at 12 days after shutdown. Subsequently, the source was used in a gamma transport simulation, with rotation applied to sample particles from an opened door. This was important since the side of the door facing the plasma will be more activated compared to the far side facing the PC. After opening the door, that activated side will be facing the port walls. This transformation of the source helped simulate a realistic situation of the open door, where the back side of the door will provide some shielding for the workers accessing the maintenance corridor. Figure 13 shows a mapping of the SDDR at 12 days from the open door only. The MCNP relative error is less than 5% in the PI.

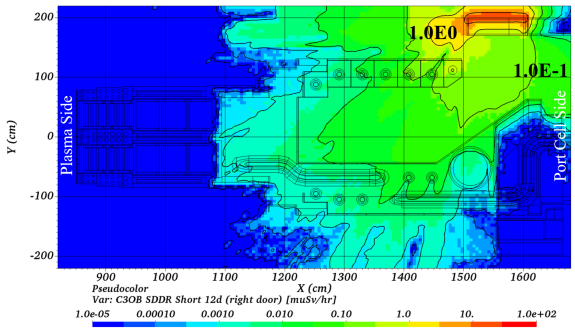

Fig. 13. C3OB SDDR [μSv/hr] around Activated Open BP Door

Secondly, using the material swapping capability in D1SUNED code, it was possible to simulate the BP in two configurations - closed during neutron transport and open for decay gamma transport - on the same simulation. That was achieved by switching material assignment of the open and closed door cells. No decay gammas were sampled from the door during this step, since the door decay gamma source was simulated in the first step separately. By adding the SDDR results from both steps, it was possible to map the total SDDR in the PI for the access configuration, C3OB, as shown in figure 14. The MCNP relative error is less than 10% in the PI.

Also, the values of the six human-sized tallies are listed in table VI.

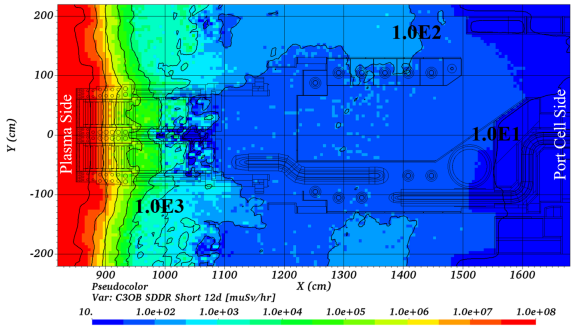

Fig. 14. C3OB SDDR [μSv/hr] at 12 Days after Shut Down

By comparing figures 11 and 14, the main difference can be found around the BP door, the upper right corner of the figures. In C3RA the SDDR levels behind the door were less than 10 μSV/hr while with the door open it goes up to about 40 μSV/hr. This is due to decay gammas coming from activated components in the PI and is a direct measure of the efficacy of the closed door in shielding the PC area behind the BP. This same conclusion can be reached using tallies 5 and 6 in table VI. With the door open, the SDDR at tally 6 goes up to about 8 μSV/hr. On the other side of the door, in the PI, the contribution of the activated door can be deduced by comparing tally number 5. Shielding the activated side of the door, with the door opened and facing the port walls, the SDDR goes down by about 7 μSV/hr.

VI.B. PF Transport

The SDDR was also calculated around the activated PF at 12 days after shut down. This is to simulate an extracted PF, with the attached central BP, in the gallery which is expected during maintenance operations. To achieve that, the neutron transport was performed in C3RA configuration. During gamma transport, the cooling water and LiPb were drained out and all the surroundings of the PF were voided in the model. This was done using the material swapping capability in D1SUNED code. Figure 15 shows a mapping of the SDDR around an extracted PF. As expected, the highest SDDR levels will be encountered inside the PF, along the maintenance corridor. This is caused by decay gammas emitted from activated components which will be surrounding a worker standing in the maintenance corridor.

The SDDR levels are nearly halved around the PF, on the outside, and the lowest are

encountered behind the central BP. This is caused be a lower activation of the far side of the central BP as neutrons suffer heavy attenuation in traversing it. The values of the six human-sized tallies along the maintenance corridor are listed in table VIII, under the "PF" column. In comparison to table VI, more than half of the contribution in C3RA configuration comes from the PF alone for tallies 2, 3, and 4. For tally number 5, equal contribution can be found from the PF itself and the surroundings. It is then recommended to take into account that region behind the BP since the shadow of the central BP can provide a proper location to set up tools or increase working time to do maintenance activities around the PF, should it be not an option to transfer a component away from the PF.

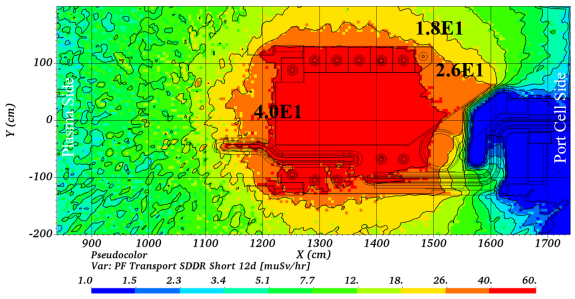

Fig. 15. SDDR [μSv/hr] at 12 Days around Activated PF in Gallery

VII. BASELINE CONFIGURATION: SDDR BREAKDOWN

In table VIII, the SDDR at the six human-sized tallies, along the maintenance corridor, are listed. The "PF" column refers to SDDR from the PF only, while the ""Non-PF" column lists the contributions from the surrounding ports, the peripheral BP, as well as the TBM-PP. At the interface between the TBP-PP and the PF, tally 1, the major contribution comes from non-PF components. This is expected since the TBM-PP will see higher neutron flux levels, being closer to the plasma. The situation is then switched for tallies 2 - 4, where inside the maintenance corridor the majority of decay gamma will be coming from the surrounding PF components. The contribution of the surrounding ports is diminished by the PF structure. For tally 6, which is located at a threshold and sees the maintenance corridor at an angle while being exposed to the neighboring ports, equal contribution is found between PF and non-PF components..

A 0.1 mm residual layer of activated LiPb in the PF would cause an increase by half in the SDDR. The largest increase is seen near the crowded pipe work of the LiPb circuit close to the

BP door, tally 4. Behind the BP, the contribution is all attributed to LiPb since the pipes exit the BP and decay gammas are emitted unattenuated. It is worth noting that the total SDDR lacks the contribution from Activated Corrosion Products (ACP) in the cooling pipes. From a recent analysis [16], using the same PF but with the model of the TBM-set, instead of the TBM-PP with dummies used in this paper, it was found that ACPs contribute as much as the activated components due to ^{17}N decay neutrons, except for the delay tank itself.

TABLE VIII
C3RA SDDR [μSv/hr] at 12 Days after Shut Down

Tally No.	**Plasma Neutrons**			**^{17}N Decay Neutrons**	**Total**
	Activated Components		**Residual 0.1 mm LiPb Layer**	**Activated Components**	
	PF	**Non-PF**			
1	24.78	45.90	39.69	0.11	110.47
2	48.49	29.95	27.70	0.09	106.23
3	52.27	27.60	35.43	0.09	115.40
4	44.22	17.68	58.58	0.09	120.57
5	21.02	19.41	35.91	0.10	76.43
6	0.01		6.94	0.00	6.95

VIII. CONCLUSIONS

In this paper, the results of scoping nuclear analyses of the evolved PF and BP were discussed. Several shielding options were investigated. It was demonstrated that combining adding B_4C panels on the internal and external of the PF structure along with lining the pipe penetration in the central BP reduces the neutron flux in the maintenance corridor as well as behind the BP. This approach has two attractive advantages: reducing activation of components in the PF, hence lower SDDR in the maintenance corridor, and also meeting the flux limits behind the BP. To protect the electronic equipment in the PI, the contribution from neutrons and gammas to the dose in Si were investigated. It was found that the major contributor was ^{16}N decay gammas. Attention was also paid to the SDDR and the efficacy of the different shielding options were compared, with a demonstrated advantage of the same approach introduced earlier. The contribution to the SDDR was investigated from different sources, activated components and residual LiPb in pipes. The SDDR in the PI was found to be above 100 μSv/hr with one third of the contributions coming from an assumed 0.1 mm residual LiPb layer.

ACKNOWLEDGMENTS

This work was funded by the ITER Organization (IO) under contract IO/19/CT/4300001953. The views and opinions expressed herein do not necessarily reflect those of IO.

REFERENCES

[1] L. Giancarli, *et al*, "ITER TBM Program and associated system engineering," *Fusion Engineering and Design*, **136**, 815 (2018); 10.1016/j.fusengdes.2018.04.014.

[2] "ITER," URL https://www.iter.org/proj/inafewlines.

[3] IAEA, "Technical Basis for the ITER Final Design Report, Cost Review and Safety Analysis (FDR)," *ITER EDA Documentation Series*, **16** (1998).

[4] M. Harb, *et al*, "Neutronics analysis and assessment of shielding options of pipe forest and Bioshield-Plug design for ITER TBSs," *Fusion Engineering and Design*, **168** (2021).

[5] D. Leichtle, *et al*, "Progress in nuclear analyses of the ITER TBM Port Plug with Dummy TBMs," *Fusion Engineering and Design*, **146**, 1574 (2019); 10.1016/j.fusengdes.2019.02.131.

[6] X-5 MONTE CARLO TEAM, "MCNP - A General Monte Carlo N-Particle Transport Code Overview and Theory Version 5 Vol. I," *Los Alamos National Laboratory, Report LA-UR-03-1987* (2003).

[7] D. Leichtle, *et al*, "The ITER tokamak neutronics reference model C-Model," *Fusion Engineering and Design*, **136**, 742 (2018); 10.1016/j.fusengdes.2019.02.131.

[8] E. Polunovskiy, "C-model R181031 model document," *IO Internal Document* (2019).

[9] P. Sauvan, "Generic C-Model with integrated neighboring ports of EP # 16," *Personal Communication* (2019).

[10] P. Sauvan, *et al*, "D1SUNED system for the determination of decay photon related quantities," *Fusion Engineering and Design*, **151 (2020)**; 10.1016/j.fusengdes.2019.111399.

[11] "Conversion Coefficients for use in Radiological Protection against External Radiation," *ICRP Publication 74, No. 3/4*, **26** (1996).

[12] "ADVANTG — An Automated Variance Reduction Parameter Generator," *ORNL/TM-2103/416, Oak Ridge National Laboratory* (2013).

[13] "MARCONI SuperComputer in CINECA," URL https://wiki.u-gov.it/confluence/display/SCAIUS/HPC+User+Guide.

[14] J. Sublet, *et al*, "The FISPACT-II User Manual," *CCFE-R (11) 11* (2014).

[15] J. van der Laan, "Average production rates of nitrogen isotopes in the TBM-PP," *Personal Communication* (2019).

[16] P. Sauvan, *et al*, "WCLL-TBS Conceptual Design. Part A: Area of Design Activities for the TBM Set (PMI-7.1.1.Phase II - Task 3 Nucl-T004-D001 (D9))," *F4E Internal Document* (2020).